Nat. Hazards Earth Syst. Sci. Discuss., 2, 6033–6067, 2014
www.nat-hazards-earth-syst-sci-discuss.net/2/6033/2014/
doi:10.5194/nhessd-2-6033-2014
© Author(s) 2014. CC Attribution 3.0 License.

Natural Hazards and Earth System Sciences
Open Access
Discussions

This discussion paper is/has been under review for the journal Natural Hazards and Earth System Sciences (NHESS). Please refer to the corresponding final paper in NHESS if available.

Numerical simulation of a winter hailstorm event over Delhi, India on 17 January 2013

A. Chevuturi[1], **A. P. Dimri**[1], **and U. B. Gunturu**[2]

[1]School of Environmental Sciences, Jawaharlal Nehru University, New Delhi, India
[2]King Abdullah University of Science and Technology, Thuwal, Saudi Arabia

Received: 6 August 2014 – Accepted: 4 September 2014 – Published: 24 September 2014

Correspondence to: A. P. Dimri (apdimri@hotmail.com)

Published by Copernicus Publications on behalf of the European Geosciences Union.

Abstract

This study analyzes the cause of rare occurrence of winter hailstorm over New Delhi/NCR (National Capital Region), India. The absence of increased surface temperature or low level of moisture incursion during winter cannot generate the deep convection required for sustaining a hailstorm. Consequently, NCR shows very few cases of hailstorms in the months of December-January-February, making the winter hail formation a question of interest. For this study, recent winter hailstorm event on 17 January 2013 (16:00–18:00 UTC) occurring over NCR is investigated. The storm is simulated using Weather Research and Forecasting (WRF) model with Goddard Cumulus Ensemble (GCE) microphysics scheme with two different options, hail or graupel. The aim of the study is to understand and describe the cause of hailstorm event during over NCR with comparative analysis of the two options of GCE microphysics. On evaluating the model simulations, it is observed that hail option shows similar precipitation intensity with TRMM observation than the graupel option and is able to simulate hail precipitation. Using the model simulated output with hail option; detailed investigation on understanding the dynamics of hailstorm is performed. The analysis based on numerical simulation suggests that the deep instability in the atmospheric column led to the formation of hailstones as the cloud formation reached upto the glaciated zone promoting ice nucleation. In winters, such instability conditions rarely form due to low level available potential energy and moisture incursion along with upper level baroclinic instability due to the presence of WD. Such rare positioning is found to be lowering the tropopause with increased temperature gradient, leading to winter hailstorm formation.

1 Introduction

An unusual winter hailstorm occurred over National Capital Region (NCR)/New Delhi, India on 17 January 2013 (16:00–18:00 UTC). Figure 1 shows satellite image of extensive cloud cover over the north Indian region during this time. Heavy precipitation was

NHESSD
2, 6033–6067, 2014

observed over north Indian region including some parts of western Himalayas. In NCR and surrounding regions along with severe rainfall there was freak hail incidence also. Table 1 corresponds to the summary of hailstorm cases over NCR (NNDC-CDO, 2013). Primarily, the Indian climate is divided into four seasons; pre-monsoon (March-April-May), monsoon (June-July-August-September), post-monsoon (October–November) and winter (December-January-February) (Attri and Tyagi, 2010). With such a classification, a pattern is observed, where most hailstorms cases over NCR dominate during the warmer periods of pre-monsoon and monsoon months. It is seen that no hailstorm cases occurred during months of February and October whereas a very few hailstorm cases occur during the winter months. Out of the 33 hailstorm cases only 5 occur during the colder/winter period; with January showing only 2 cases. Thus, winter hailstorms can be considered a rare occurrence over NCR. With such a distinction between summer and winter hailstorms, it can be hypothesized that the mechanisms of these two kinds of hailstorms are different, which are deliberated in the following paragraphs.

Over north Indian region, pre-monsoon storm events occur during convectively unstable atmospheric conditions culminating due to transient disturbances observed in the air mass due to the surface heating. Storms may be categorized as severe storms if it is associated with hail, thunder, lightning, high winds etc (Houze Jr., 1981). These severe storms occur during strong vertical wind shear, which are ideal conditions for hail formation (Orville and Kopp, 1977). During monsoon, the precipitation is caused due to development of deep convection because of higher surface temperature and vertical wind shear of south-westerly flow and associated moisture incursion over the Indian subcontinent. The convective precipitation is also facilitated by surface terrain and the Himalayan orography. These periods of precipitation occurrences during the monsoon are associated with rainfall and in extreme cases hail (Koteswaram, 1958; Ramage, 1971; Sikka, 1977; Lau et al., 2012). In the context of hailstorms, it can be concluded that convection due to high surface temperatures and moisture laden flow are important for hailstorm formation. Hail is precipitation in the form of hard, rounded

NHESSD
2, 6033–6067, 2014

pellets of irregular lumps of ice. In cross section, hail shows concentric shells of different densities and degrees of opaqueness (Pruppacher and Klett, 2010). These multiple layers of ice within hail are formed due to continuous deposition and shedding of ice over the condensation nuclei as the hailstones cycle through strong convective clouds having multiple updrafts and downdrafts (Chatterjee et al., 2008).

The winter months are associated with absence of increased surface temperatures or low level of moisture incursion, making it a cold and dry season (Attri and Tyagi, 2010). These conditions are not conducive for generation of deep convection required for sustaining a hailstorm. In month of January the average temperature of Delhi is 13.5 °C (NNDC-CDO, 2013). With such low mean temperature, it is difficult for a storm to attain the wind shear required for hail formation. Studying such unusual/abnormal meteorological condition conducive for winter hail formation is of interest. Thus, this study has a new and unique perspective to understand the dynamics of a winter hailstorm occurrence. Though hailstorms are a rare phenomenon due to very specific conditions of formation and subsequent occurrence (Table 1), they are quite hazardous. Hailstones destroy crop, infrastructure, property and in extreme cases may cause injuries to humans (De et al., 2005). Due to the perspective of hailstorms happening only in summer, hailstorms are not expected in winter months. This may lead to unpreparedness in early warning systems for hail prediction and mitigation of damage due to hailstorms, which may lead to devastating consequences.

Numerical weather prediction technique is utilized for understanding the above discussed storm event. This storm is simulated with Weather Research and Forecasting (WRF) model with Advanced Research WRF (ARW) dynamical core. As hail formation is a microphysical process, the study mainly focuses on the use of Goddard Cumulus Ensemble (GCE) (Lin et al., 1983; Rutledge and Hobbs, 1984; Tao and Simpson, 1993) microphysics scheme to simulate hail formation. This scheme simulates six different hydrometeors or water particles: water vapour (WV), cloudwater (CW), cloudice (CI), rainwater (RW), snow and a third class of ice. The third class of ice can be graupel or hail as per the options used during simulation. Graupel is relatively smaller and

NHESSD
2, 6033–6067, 2014

less dense hydrometeor ice particle when compared with hail. These variations cause differences in microphysical properties of the model parameterization. This study includes analysis of simulations with both options of GCE microphysics for the hailstorm event, which will hereafter referred to as hail option or graupel option.

With these considerations, the objectives of this study are listed below:

- To understand and describe a winter hailstorm event over NCR, with discussion on the large scale flow and precipitation associated during such storms.
- To simulate the hailstorm event using GCE microphysics scheme's hail and graupel options for a comparative analysis in the two options.
- To study in detail the various thermodynamic and microphysical processes associated with the hailstorm formation using the GCE microphysics with hail option.

This paper is divided into the following sections with Sect. 2 describing experimental design and data, Sect. 3 showing results and discussion and summary and conclusion provided in Sect. 4.

2 Experimental design and data

In this study, the WRF model (version 3.0) with the ARW dynamic solver is used to simulate the hailstorm event. The WRF model is a mesoscale dynamical model, developed by a multi-institutional collaboration (Wang et al., 2010) including the National Oceanic and Atmospheric Administration (NOAA), USA and the National Center for Atmospheric Research (NCAR), USA. The ARW dynamic solver (Skamarock et al., 2008) is developed primarily at NCAR. The model domain is set up over India with a central domain point at NCR (28.6° N 77.2° E), where the high intensity precipitation was reported, with four nests of 27 km, 9 km, 3 km and 1 km respectively (Fig. 2 and Table 2). Model simulations are analyzed for 72 h starting from 00:00 UTC 16 January

NHESSD
2, 6033–6067, 2014

2013, to understand the meteorological processes contributing to the storm development and propagation. In the current study, not only model performance in simulating the precipitation event is evaluated for verification, but the large scale atmospheric processes leading to the weather event are also analyzed. With such an aim, a three day simulation is deemed necessary for the study.

NCEP Final analysis data (FNL), at $1^{\circ} \times 1^{\circ}$ spatial resolution, is used as the initial and lateral boundary conditions for the study (NCEP/NOAA/US-DoC, 2000). Initial conditions for the model are extracted from the FNL dataset and are interpolated to the model domain. NASA's Modern Era Retrospective-analysis for Research and Applications (MERRA) (Rienecker et al., 2011) 6 hourly analysis dataset with a spatial resolution of $0.5^{\circ} \times 0.7^{\circ}$ is used as corresponding observational data. Tropical Rainfall Measuring Mission (TRMM) multi-satellite precipitation analysis (real time data) 3B42 V7 (Huffman et al., 2007) at $0.25^{\circ} \times 0.25^{\circ}$ spatial resolution is used as the observation for the precipitation fields. The daily OLR (Liebmann and Smith, 1996) dataset provided by Earth Systems Research Laboratory (ESRL), National Oceanic and Atmospheric Administration (NOAA), USA, available at $2.5^{\circ} \times 2.5^{\circ}$ spatial resolution is used for validation purposes.

As discussed previously the GCE microphysics scheme (Tao and Simpson, 1993) is used in the model simulation experiments. This parameterization scheme is based on the multi-dimensional, non-hydrostatic microphysics cloud resolving model (Simpson and Tao, 1993). The microphysics scheme simulates six different hydrometeors: WV, CW, CI, RW, snow and the third class of ice (which can be either hail or graupel, as specified). The two options are different due to different microphysical processes considered for hail/graupel formation, which in turn impact the hydrometeor population. As both the hydrometeors are quite alike, their formation processes considered in both options of the parameterization scheme are similar; accretion of RW, aggregation of snow, rimming of CI, sublimation and melting (Lin et al., 1983). But with graupel option, two other processes are included for graupel formation; autoconversion of snow and deposition of WV (Rutledge and Hobbs, 1984). In this study to understand the

NHESSD
2, 6033–6067, 2014

microphysical process of hail formation and its complexities, simulation is conducted using the hail option specifically. It is to be mentioned that both simulations 3 and 1 km resolution nests were simulated with explicit representation of cumulus parameterization scheme. As model for simulations at horizontal resolutions smaller than 3 km, estimates the precipitation by the cloud microphysics scheme itself (Gomes and Chou, 2010).

3 Results and discussion

3.1 Analysis of large scale flow and precipitation

The model simulated large scale flow patterns at 500 hPa and its corresponding MERRA observation is depicted in Fig. 3. The large scale circulation showed a deep trough being formed over the western Indian and Pakistan region in model fields and corresponding MERRA observational analysis. Figure 3 depicts that both the model simulations capture the wind and geopotential height patterns with slight over estimation. The depression observed over the region corresponds to an incoming western disturbance (WD). WDs are eastward moving synoptic scale extra-tropical cyclonic systems in the sub-tropical westerly jet. These originate in the Mediterranean Sea and cause precipitation over northern India mainly during the months of December-January-February, due to their interaction with the Himalayan orography (Dimri, 2004). This migratory disturbance in the mid-troposphere along with the stationary surface low over western India is called the WD, and generates the instability necessary for winter precipitation (Dimri and Chevuturi, 2013). The presence of this system can be the cause for the enhanced the instability over the region that influences the storm formation.

Daily mean outgoing longwave radiation (OLR) for 17 January 2013 is depicted in Fig. 4 for model simulations and corresponding observation. A clear region of low OLR values is seen over whole of northern India including the NCR in both model options

NHESSD
2, 6033–6067, 2014

and observations. OLR can be considered as an indicator to describe the clouding condition or precipitation globally (Xie and Arkin, 1998). In the presence of increased extent and depth of cloud cover and lower cloud top temperatures in high clouds, low OLR values are recorded. Thus, the figure represents the cloud extent during the time period of the hailstorm. On evaluating the satellite image of Fig. 1, similar cloud extent is observed over the same region. The low values of OLR over the whole of northern Indian region depict extensive cloud cover and the possibility of precipitation over the region. The advance of WDs and interaction with Himalayas is associated with the development of mesoscale cloud formation (Puranik and Karekar, 2009) as seen during this event. Moisture flux transport and divergence integrated over the vertical atmospheric column for observation and model simulations is shown in Fig. 5. In model simulated outputs, a strong region of moisture convergence is seen over NCR and some parts of Himalayan region north of NCR. Corresponding observations show a similar extent of moisture convergence zone, but the strength of moisture convergence is lower. According to the figure, it is observed that Arabian Sea and Bay of Bengal are both sources of moisture for the convergence zone. The moisture laden flow from these sources flows over the Indian subcontinent, congregates and flows towards NCR. This moisture is important for the maintenance of the winter storm over northern India and its role will be discussed later in detail.

Analysis of three hourly precipitation rate from model simulations and its corresponding observation is shown in Fig. 6. The figure suggests that there was a storm having maximum intensity over NCR between 15:00 to 18:00 UTC of 17 January 2013. This storm showed a localized formation over NCR and its surrounding region. When compared with the observation, model simulated output shows a similar spatial extent of precipitation patterns. The axis of the storm evolution is observed to be oriented along north-east to south-west direction. On evaluating the two model simulations, it is observed that hail option shows closer precipitation intensity with TRMM observation than the graupel option. The spatial extent of precipitation pattern observed in hail option is also better match when compared with the observational analysis. Figure also depicts

NHESSD
2, 6033–6067, 2014

that storm cluster moves eastward as the storm progresses. The analysis shows localized cluster of storm that is the cause of the heavy precipitation event. But when the point specific precipitation intensity at NCR is compared between the different options, overestimation is observed in model simulation. Inter-comparison in temporal variation in half hourly precipitation intensities of both model simulations is shown in Fig. 7 for all four horizontal model resolutions. The figure suggests peak concentration of precipitation around NCR region was observed around 17:00 UTC on 17 January 2013. Here it is also clearly noted that hail option shows higher precipitation estimates than the graupel option. Deliberations on reasons for variation in precipitation intensities within the options of microphysics are provided in next section by comparative analyses of the flux in the different hydrometeors in different options.

3.2 Comparative analysis between hail and graupel options of GCE microphysics

Figure 8 depicts the mixing ratios of different hail and graupel outputs over spatial and temporal scales for both hail and graupel options. Increased concentrations of mixing ratios of all six hydrometeors are observed over the NCR region around the peak of the storm (Supplement; Figs. S1–S5). These hydrometeors are indicators of cloud formation over the region. All the hydrometeor mixing ratio concentrations show higher values over NCR around 16:30 UTC, which is just before storm peaks representing storm evolution and/or build-up. In hail option, the increased formations of hydrometeors are specifically observed over NCR, whereas some displacement is seen in graupel option output. In addition, the spatio-temporal variation of these mixing ratios shows an eastward movement of the storm. The increase of WV in the atmospheric column is due to the moisture incursion from the Arabian Sea and Bay of Bengal. As the WV rises in the atmosphere, formation of CW and CI begins by condensation and deposition processes due to decreasing temperatures, which form the clouds. The CW droplets are suspended in the atmospheric column in the mid-tropospheric layers, whereas CI particles are found in upper-troposphere where much colder conditions prevail. The RW

NHESSD
2, 6033–6067, 2014

droplets formation is enhanced by the processes of collision and coalescence (Oriville and Kopp, 1977), and ultimately sediment out as rain. Increased RW mixing ratios are an indicator of increased precipitable water availability in the atmospheric column. With the development of stronger storm conditions, there is formation of other hydrometeors like snow, hail and graupel. With the main focus of the paper on the third class of ice, we will be discussing hail and graupel in more detail.

Hail and graupel are both ice particles seen during storm formation. Hail is an ice particle which is formed due to consecutive processes like soft hail processes (dry growth and raindrop freezing) or hard hail processes (wet growth and shedding) (Wisner et al., 1972). These continuous and repeated processes form a differentially layered ice precipitation type called hail (Pruppacher and Klett, 2010). The hailstones grow as the ice particles cycle through multiple cells of convective clouds (Chatterjee et al., 2008). Graupel are similar but smaller ice particles with a diameter less than 5 mm, formed exclusively by soft hail processes (Pruppacher and Klett, 2010). In the model simulation peak hail mixing ratios are observed over NCR around 16:00–16:30 UTC, whereas graupel mixing ratios maxima is seen east of NCR. In the vertical profile hail mixing ratios span from 800–200 hPa whereas graupel mixing ratios show extent from 750–300 hPa. It is interesting to note that when hail and graupel mixing ratios are compared, the hail mixing ratios are lower than graupel mixing ratios. But graupel precipitation or sedimentation is not observed in the model simulation but hail precipitation is observed in the hail option around NCR between 16:30–17:00 UTC as shown in Fig. 9. This observation can be attributed to the fact that graupel have high number concentrations in the atmospheric column as these small ice particles are formed much quicker than hailstones. But due to their small size the graupel particles also melt quicker due to the temperature conditions that are not as low as seen over the snowline. Thus, sedimentation of graupel is not observed over NCR but hail precipitation is seen during this hailstorm. With this discussion it can be concluded that to understand hail formation over NCR, microphysics with hail option needs to be studied in depth. Subsequent section focuses on understanding the cause of winter hailstorm formation.

NHESSD
2, 6033–6067, 2014

3.3 Detailed analysis of winter hailstorm formation

For a focused analysis of the winter hailstorm formation the time period of peak precipitation 17:00 UTC 17 January 2013 is considered (Fig. 10). Vertical cross sections of various parameters analyzed along the axis of core precipitation zone of the storm region as demarcated by a green line Fig. 10. Some of the model simulated fields are also evaluated by considering their area averaged values over the 1° × 1° grey box around NCR as drawn in Fig. 10. The region over and around 77.2° E and 28.6° N would be considered the NCR or the region of study/interest.

The analysis of the dynamical properties pertaining to the winter hailstorm along the axis demarcated in Fig. 10 is provided in Fig. 11. Model simulates a region of high equivalent potential temperature (EPT) over the NCR, as seen in the Fig. 11a. This represents higher temperatures and moisture content in the mid-troposphere whereas in lower troposphere decreased EPT is noticed. This represents the region of instability spanning the atmospheric column which is the cause of the storm. The instability in the mid-tropospheric level is caused by the WD depression as observed at 500 hPa. In this region, vertical wind (Fig. 11a) shows cells with updraft and downdraft conditions. Hailstorms forming processes are known for multiple cellular structure showing regions of updrafts and downdrafts within the cloud, with dynamic movement and reflectivity patterns. The updrafts originate from the air inflow from the surface towards the cloud in the opposite direction of storm movement (Chalon et al., 1976). Whereas, the downdraft cells are caused by the air that ascends in the updrafts, and ultimately flows as outflow of air towards the front and back of the storm movement (Frankhauser, 1976; Strauch and Merrem, 1976). Relative vorticity and divergence in Fig. 11b, show alternative cells of positive and negative relative vorticity over NCR, which correspond to cyclonic and anti-cyclonic circulation respectively. These cells represent a gradient of vorticity, depicting a positive vorticity advection which culminates in rising air. Associated to these cells are regions of divergence and convergence. The convergence zone observed in the mid-tropospheric level corresponds to the multiple cells of the

NHESSD
2, 6033–6067, 2014

hailstorm. These define the movement of hydrometeors through the associated updrafts and downdrafts. As discussed above, the multiple cells formed in the clouds promote the formation of hailstones. Further, positive specific humidity anomaly over NCR is observed in the mid-troposphere (Fig. 11c). This indicates that the atmospheric column over NCR upto 200 hPa shows a high moisture zone. This increased level of moisture is required for not only growth of rain drops but also for diffusional and accretional growth of the hailstones. With the evolution of the storm, there is increase in different hydrometeors as discussed above. This indicates increase in reflectivity during storm formation (Fig. 11c). The storm shows increase of RW droplets, which congregate in the lower levels of atmosphere, showing high reflectivity values in the same region. The positive reflectivity values do not extend beyond 600 hPa, showing that this winter hailstorm does not have the deep convection as observed in tropical summer thunderstorms. So the question of cause of hailstorm formation during this storm still remains.

To understand the reason for development of instability driving the winter hailstorm, the geopotential height over the region is studied (Fig. 11d). Over NCR the geopotential height anomaly shows an increase around 400–200 hPa. This increase is associated with the dipping in the perturbation geopotential height contour lines. These changes are due to the tropopause fold penetrating the troposphere. The dip in the tropopause height values is also observed in the station data over New Delhi (Source: university of Wyoming, Sounding data). This tropopause lowering is associated with baroclinic instability occurring over the region (Bush and Peltier, 1994). The increase storm intensity over the region is caused by the baroclinic instability due to the passing WD and the development of cyclonic circulation. The mid-latitude migratory WD attains higher intensities in form of a baroclinically unstable disturbance specifically over Indian region (Rao and Rao, 1971; Singh and Agnihotri, 1977). This instability in the mid- to upper tropospheric levels generates the turbulent convective energy required for the development of updrafts during storm occurrence. With the availability of moisture in the atmospheric column the instability leads to heavy precipitation. But a WD

NHESSD
2, 6033–6067, 2014

over northern India does not always lead to hail formation during winter. Hail precipitation in model simulation is seen from 16:00–17:00 UTC 17 January 2013 (Fig. 9). The updrafts driven by the instability developed over the region, cycles the hail through the cloud. Hail particle successively moving through the vertical column grows in the upward motion and melts/sheds in the downward movement. With each cycle the hailstone grows a new layer of ice forming the concentric circles seen in a hailstone cross section as discussed above. Thus, vertical wind velocity is an important factor for the hail formation. Heymsfield et al. (2005) describes that strong convective updrafts (with vertical wind speed greater than 5–10 m s^{-1}) suppress homogenous nucleation to form ice particles which grow to form hail. Whereas, lower wind speeds would not attain enough energy to develop a strong hailstorm. The model simulated vertical wind updraft speeds over NCR show a magnitude of 4–6 m s^{-1} which provide sufficient time for ice particle growth by dry or wet growth.

The instability developed in the mid-tropospheric levels due to the WD develops propensity for baroclinic atmosphere in the upper half of troposphere. When the temporal variation of temperature profile of the region is analyzed, a dip is observed in the −60 °C isotherm around 16:00–17:00 UTC (Fig. 12). This lowering corresponds to the troposphere fold discussed before. The lowering of tropopause causes incursion of colder stratospheric layers into warmer troposphere. This in turn causes development of a steep temperature gradient as seen in the figure, which enhances upper level instability. Still the reasons for instability in the lower layers are yet not clearly discussed. To understand the lower layer instability, temporal variation in area averaged convective available potential energy (CAPE) and specific humidity are represented in black and blue contours of Fig. 12 respectively. In this figure, an increase of moisture over NCR in the lower levels of atmospheric column is observed along with development of CAPE from around 13:00 UTC. The source of this low level moisture incursion is majorly from Arabian Sea and on a lesser extent from Bay of Bengal (Fig. 5). The moisture convergence develops buoyancy which enhances the propensity of increase of CAPE in the atmospheric column. There is reduction in CAPE values in subsequent time periods

NHESSD
2, 6033–6067, 2014

after 13:00 UTC. The increase of CAPE defines the potential energy that is available to drive a storm and release of CAPE in form of kinetic energy promotes storm development. Along with this the low level moisture incursion provides the buoyancy required for the air parcel to rise. Thus, upper level instability is predominantly by the existing WD embedded with the low level instability due to moisture incursion and development of CAPE lead to instability spanning the troposphere which makes it conducive conditions for hailstorm formation. Muller et al. (2008) and Rosenfeld and Lensky (1998) described the "continental" clouds having three zones in the vertical direction based on temperature variation: diffusional droplet growth zone (upto −10 °C), mixed phase zone (−10 to −38 °C) and glaciated zone (above −38 °C). The isotherm of −38 °C is termed as homogeneous freezing isotherm beyond which homogenous nucleation occurs. As per Fig. 12, it can be concluded that the mixed phase zone for the current hailstorm can be considered within 600–350 hPa. The mixed phase zone is the region for development of hail particles due to growth by deposition of water particles. This zone in the model simulated output coincides with region having strong convergence influence and higher specific humidity, promoting hail formation along with raindrop growth. The region of glaciation in the upper levels of troposphere is imperative for the development of small ice particles through homogenous nucleation. These particles further grow to form the various ice precipitation forms, in this case hail. The problem with winter storms is that instability is not sufficient enough for the cloud to extend to this height or form an anvil. But in the 17 January 2013 hailstorm, the instability extending from low to upper levels of troposphere discussed above allows the formation of ice nuclei in the glaciations zone leading to winter hail formation.

The clarity of two different zones of instability can be described in the sounding data of NCR for 17 January 2013. Figure 13 represents the model and observed sounding data in a graphical format. The development of instability at 12:00 UTC is an indicator for the storm development. This instability is measured by the gap between the air parcel lapse rate and environmental lapse rate. There is increased instability around mid-tropospheric level in both model and observation due to the approaching WD and

NHESSD
2, 6033–6067, 2014

development of baroclinic instability. Another region of higher instability seen in the observation is around 700 hPa, which is underestimated in the model simulation. This region of instability corresponding to the lower level convection described due to development of CAPE and the moisture incursion. There is augmented moisture content in the atmospheric column as seen in the relative humidity profile provides buoyancy to the air parcel. Combination of low level available potential energy and moisture incursion along with upper level baroclinic instability due to the presence of WD, led to sufficient instability for winter hail formation.

4 Summary and conclusions

This study investigates the cause of hailstorm during winter over NCR. Winter months of December-January-February, specifically over north India, are considered a cold and dry season. But high surface temperature and supplementary moisture availability are the prerequisite for hailstorm development. And winter storms are not able to attain the intensity and depth of a convective storm. Thus, the question of hail being formed during the winter season is fascinating due to its uniqueness.

The comprehensive analysis of the results has led the authors to describe the mechanism of the winter hailstorm formation over NCR. These conclusions have been summarized in the form of an illustration or conceptual model as given in Fig. 14. On the day of the hailstorm, 17 January 2013, high moisture availability is seen over NCR. *Arabian Sea* and *Bay of Bengal* are identified as the source of this moisture in-flow. This *moisture* incursion along with the release of *CAPE* in the lower levels leads to development of the *lower level instability*. But this instability is not sufficient for a winter storm. On the other hand winter precipitation is experienced over north India due to *WDs*. These migratory disturbances in the sub-tropical westerly jet cause *baroclinic instability* in the mid/upper troposphere. Thus, with two different sources of instability this winter storm is able attain conditions similar to deep convective storms favorable for hail formation.

NHESSD
2, 6033–6067, 2014

The *lower level instability* formed due to release of kinetic energy and buoyancy of air parcel due to high relative humidity. This *mid/upper level instability* develops due to lowering of the *tropopause* which intensifies the *temperature gradient*. Thus, a rising air parcel gets an enhanced push to continue rising, which denotes the formation clouds having larger vertical extents. Ice nucleation, which develops hail nuclei, is enhanced in such clouds as they attain the *glaciated zone*. These clouds are also associated with cells having turbulent upward and downward wind movement. Development of these conditions supports *cycling of hail* through the clouds and promotes its formation through shedding, deposition and other hail processes. As the hailstones grow, they ultimately sediment or precipitate out to cause the hailstorm during winter.

The Supplement related to this article is available online at doi:10.5194/nhessd-2-6033-2014-supplement.

Author contributions. A. Chevuturi, A. P. Dimri and U. B. Gunturu defined objectives and designed the experiment. A. Chevuturi carried out the simulation and prepared the results. A. P. Dimri and U. B. Gunturu were instrumental in analysis of the results and outlining the discussion. A. Chevuturi prepared the manuscript with contributions from all co-authors.

Acknowledgements. This work is partially funded by the senior research fellowship provided to A. Chevuturi by Human Resource Development Group at Council for Scientific and Industrial Research, India. Authors would like to acknowledge the use of NCEP FNL dataset as the initial and boundary conditions as input for the model simulation archived at Research Data Archive at the National Center for Atmospheric Research, Computational and Information Systems Laboratory. Authors acknowledge the Global Modeling and Assimilation Office (GMAO) and the GES DISC for the dissemination of MERRA dataset. Authors like to acknowledge GSFC/DAAC, NASA for the access of TRMM data. Interpolated OLR data used in the study is provided by the NOAA/OAR/ESRL PSD, Boulder, Colorado, USA.

References

Attri, S. D. and Tyagi, A.: Climate Profile of India, Meteorological Monograph No. Environment Meteorology-01/2010, India Meteorological Department, New Delhi, available at: http://www.imd.gov.in/doc/climate_profile.pdf (last access: 17 March 2013), 2010.

Bush, A. B. G. and Peltier, W. R.: Tropopause folds and synoptic-scale baroclinic wave life cycles, J. Atmos. Sci., 51, 1581–1604, 1994.

Chalon, J. P., Famkhauser, J. C., and Eccles, P. J.: Structure of an evolving hailstorm, Part 1: General characteristics and cellular structure, Mon. Weather Rev., 104, 564–575, 1976.

Chatterjee, P., Pradhan, D., and De, U. K.: Simulation of hailstorm event using Mesoscale Model MM5 with modified cloud microphysics scheme, Ann. Geophys., 26, 3545–3555, doi:10.5194/angeo-26-3545-2008, 2008.

De, U. S., Dube, R. K., and Rao, G. P.: Extreme weather events over India in the last 100 years, J. Ind. Geophys. Union, 9, 173–187, 2005.

Dimri, A. P.: Impact of horizontal model resolution and orography on the simulation of a western disturbance and its associated precipitation, Meteorol. Appl., 11, 115–127, 2004.

Dimri, A. P. and Chevuturi, A.: Model sensitivity analysis study for western disturbances over the Himalayas, Meteorol. Atmos. Phys., 123, 155–180, 2014.

Fankhauser, J. C.: Structure of an evolving hailstorm, Part II: Thermodynamic structure and airflow in the near environment, Mon. Weather Rev., 104, 576–587, 1976.

Gomes, J. L. and Chou, S. C.: Dependence of partitioning of model implicit and explicit precipitation on horizontal resolution, Meteorol. Atmos. Phys., 106, 1–18, 2010.

Heymsfield, A. J., Miloshevich, L. M., Schmitt, C., Bansemer, A., Twohy, C., Poellot, M. R., Fridlind, A., and Gerber, H.: Homogeneous ice nucleation in subtropical and tropical convection and its influence on cirrus anvil microphysics, J. Atmos. Sci., 62, 41–64, 2005.

Houze Jr., R. A.: Structures of atmospheric precipitation systems – a global survey, Radio Sci., 16, 671–689, 1981.

Huffman, G. J., Adler, R. F., Bolvin, D. T., Gu, G., Nelkin, E. J., Bowman, K. P., Hong, Y., Stocker, E. F., and Wolff, D. B.: The TRMM multi-satellite precipitation analysis: quasi-global, multi-year, combined-sensor precipitation estimates at fine scale, J. Hydrometeorol., 8, 38–55, 2007.

NHESSD
2, 6033–6067, 2014

Kosteswaram, P.: The Asian Summer Monsoon and the General Circulation over Tropics, The Proceeding of the International Symposium on Monsoons of the World New Delhi, 105–110, 1958.
Lau, W. K., Waliser, D. E., and Goswami, B. N.: South Asian monsoon, in: Intraseasonal Variability in the Atmosphere–Ocean Climate System, Springer, Berlin, Heidelberg, 21–72, 2012.
Liebmann, B. and Smith, C. A.: Description of a complete (interpolated) outgoing longwave radiation dataset, B. Am. Meteorol. Soc., 77, 1275–1277, 1996.
Lin, Y. L., Farley, R. D., and Orville, H. D.: Bulk parameterization of the snow field in a cloud model, J. Clim. Appl. Meteorol., 22, 1065–1092, 1983.
Muller, C. L., Kidd, C., Fairchild, I. J., and Baker, A.: Investigation into clouds and precipitation over an urban area using micro rain radars, satellite remote sensing and fluorescence spectrophotometry, Atmos. Res., 96, 241–255, 2010.
National Centers for Environmental Prediction/National Weather Service/National Oceanic and Atmospheric Administration/US Department of Commerce: NCEP FNL Operational Model Global Tropospheric Analyses, continuing from July 1999, Research Data Archive at the National Center for Atmosheric Research, Computational and Information Systems Laboratory, available at: http://rda.ucar.edu/datasets/ds083.2 (last access: 5 May 2013), 2000.
NNDC-CDO: NOAA National Data Center Climate Data Online, available at: http://www7.ncdc.noaa.gov/CDO/cdo (last access: 5 May 2013), 2013.
Orville, H. D. and Kopp, F. J.: Numerical simulation of the life history of a hailstorm, J. Atmos. Sci., 34, 1596–1618, 1977.
Pruppacher, H. R. and Klett, J. D.: Microphysics of clouds and precipitation, 2nd Edn., Atmos. Ocean. Sci. Lib., 18, Springer, New York, USA, 976 pp., 2010.
Puranik, D. M. and Karekar, R. N.: Western disturbances seen with AMSU-B and infrared sensors, J. Earth Syst. Sci., 118, 27–39, 2009.
Ramage, C. S.: Monsoon meteorology, in: Int. Geophys. Ser. 15, Academic Press, San Diego, USA, 1971.
Rao, V. B. and Rao, S. T.: A theoretical and synoptic study of western disturbances, Pure Appl. Geophys., 90, 193–208, 1971.
Rienecker, M. M., Suarez, M. J., Gelaro, R., Todling, R., Bacmeister, J., Liu, E., Bosilovich, M. G., Schubert, S. D., Takacs, L., Kim, G. K., Bloom, S., Chen, J., Collins, D., Conaty, A., da Silva, A., Gu, W., Joiner, J., Koster, R. D., Lucchesi, R., Molod, A., Owens, T.,

NHESSD
2, 6033–6067, 2014

Pawson, S., Pegion, P., Redder, C. R., Reichle, R., Robertson, F. R., Ruddick, A. G., Sienkiewicz, M., and Woollen, J.: MERRA: NASA's modern-era retrospective analysis for research and applications, J. Climate, 24, 3624–3648, 2011.

Rosenfeld, D. and Lensky, I. M.: Satellite-based insights into precipitation formation processes in continental and maritime convective clouds, B. Am. Meteorol. Soc., 79, 2457–2476, 1998.

Rutledge, S. A. and Hobbs, P. V.: The mesoscale and microscale structure and organization of clouds and precipitation in extratropical cyclones, XII: A numerical study of precipitation processes in narrow cold-frontal rainbands, J. Atmos. Sci., 41, 2949–2972, 1984.

Sikka, D. R.: Some aspects of the life history, structure and movement of monsoon depressions, Pageoph, 115, 1501–1529, 1977.

Simpson, J. and Tao, W. K.: The Goddard cumulus ensemble model. Part II: Applications for studying cloud precipitating processes and for NASA TRMM, Terr. Atmos. Ocean. Sci., 4, 73–116, 1993.

Singh, M. S. and Agnihotri, C. L.: Baroclinity over India in winter and its relation to western disturbances and jet streams – Part 1, Ind. J. Meterol. Hydrol. Geophys., 28, 303–310, 1977.

Skamarock, W. C., Klemp, J. B., Dudhia, J., Gill, D. O., Barker, D. M., Duda, M. G., Huang, X., Wang, W., and Powers, J. G.: A Description of the Advanced Research WRF Version 3, MMM, UCAR, available at: http://www.mmm.ucar.edu/wrf/users/docs/arw_v3.pdf (last access: 17 August 2012), 2008.

Strauch, R. G. and Merrem, F. H.: Structure of an evolving hailstorm, Part III: Internal structure from Doppler radar, Mon. Weather Rev., 104, 588–595, 1976.

Tao, W. K. and Simpson, J.: The Goddard cumulus ensemble model, Part I: Model description, Terr. Atmos. Ocean. Sci., 4, 35–72, 1993.

Wang, W., Barker, D. M., Bruy'ere, C., Duda, M. G., Dudhia, J., Gill, D. O., Michalakes, J., and Rizvi, S.: WRF Version 3 Modeling System User's Guide, MMM, UCAR, available at: http://www.mmm.ucar.edu/wrf/users/docs/user_guide_V3.0 (last access: 15 August 2012), 2010.

Wisner, C., Orville, H. D., and Myers, C.: A numerical model of a hail-bearing cloud, J. Atmos. Sci., 29, 116–1181, 1972.

Xie, P. and Arkin, P. A.: Global monthly precipitation estimates from satellite-observed outgoing longwave radiation, J. Climate, 11, 137–164, 1998.

NHESSD
2, 6033–6067, 2014

Table 1. Cases of the hailstorms over NCR from 1943–2013 (NNDC-CDO, 2013). The case discussed in the present study is marked with *.

Months	Cases	Dates
January	2	6 Jan 2012-01-06, 17 Jan 2013*
February	0	–
March	4	30 Mar 1957, 11 Mar 1974, 24 Mar 1975, 28 Mar 2013
April	7	3 Apr 1944, 15 Apr 1957, 18 Apr 1978, 16 Apr 1983, 22 Apr 1991, 10 Apr 1993, 22 Apr 2004
May	5	30 May 1958, 18 May 1983, 5 May 1994, 9 May 1994, 11 May 1996
June	3	4 Jun 2000, 24 Jun 2000, 23 Jun 2004
July	2	16 Jul 2000, 24 Jul 2000
August	5	31 Aug 1986, 20 Aug 2005, 14 Aug 2006, 25 Aug 2009, 24 Aug 2011
September	2	20 Sep 1975, 12 Sep 1984
October	0	–
November	1	10 Nov 1973
December	2	23 Dec 1977, 29 Dec 1990
Total	33	

NHESSD
2, 6033–6067, 2014

Table 2. Description of model details.

Model	WRF Version 3.0
Map Projection	Mercator
Horizontal Resolution	Nest: 27 km, 9 km, 3 km, and 1 km
Hailstorm Case Simulation	00:00 UTC 16 Jan 2013 to 00:00 UTC 19 Jan 2013
Central Point of Domain	28.6° N 77.2° E
Horizontal Grid Scheme	Arakawa C-grid
Time Step	162 s
Microphysics	GCE Scheme (with HAIL OPTION)
Land surface model	Noah Land Surface Model
Surface layer model	MM5 Similarity Model
Radiation Scheme	Shortwave – Dudhia Scheme Longwave – RRTM
Planetary boundary layer	Mellor–Yamada–Janjic scheme
Cumulus Parametrization	Kain–Fritsch Scheme

NHESSD
2, 6033–6067, 2014

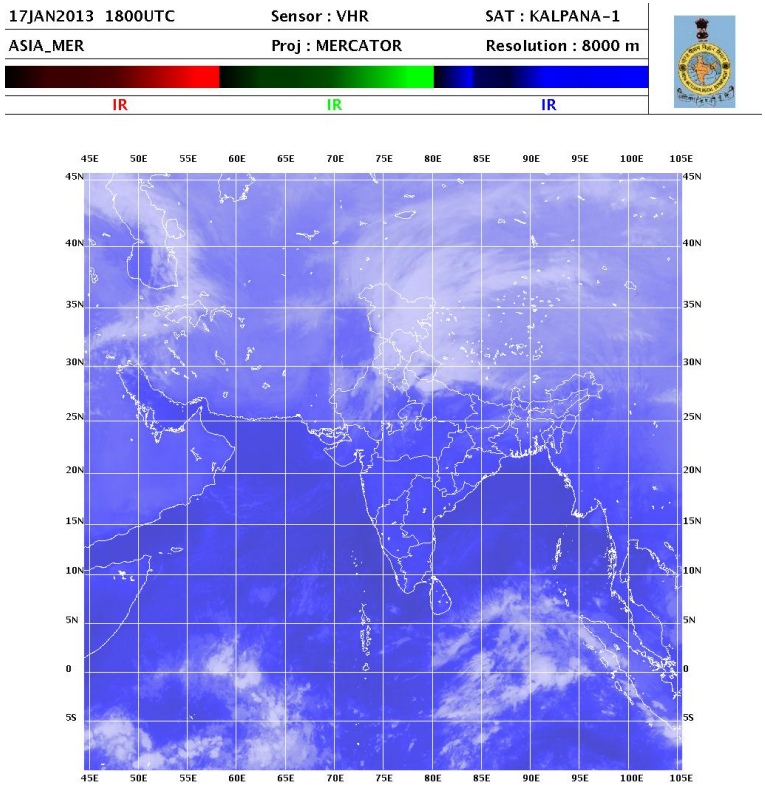

Figure 1. Kalpana-I satellite image for 18:00 UTC 17 January 2013 with VHR sensor over Asia with Mercator projection (source: http://www.imd.gov.in/section/satmet/dynamic/insat.htm).

NHESSD
2, 6033–6067, 2014

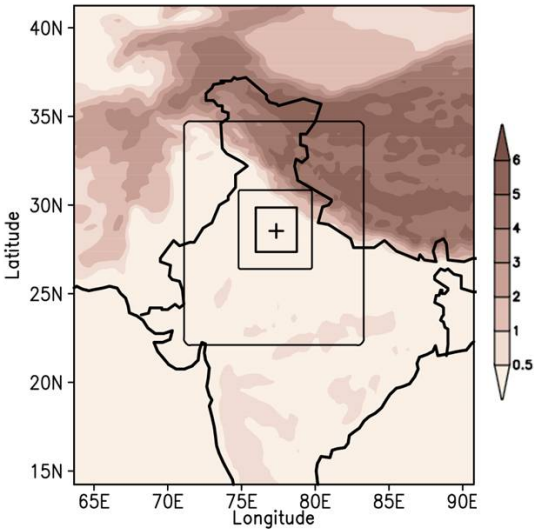

Figure 2. Model domain and topography ($\times 10^3$ m; shaded). Shaded region corresponds to model domain 1 (27 km horizontal model resolution), and boxes with solid black lines indicate model domain 2 (9 km horizontal model resolution), domain 3 (3 km horizontal model resolution), and domain 4 (1 km resolution). + Sign indicates location of NCR.

NHESSD
2, 6033–6067, 2014

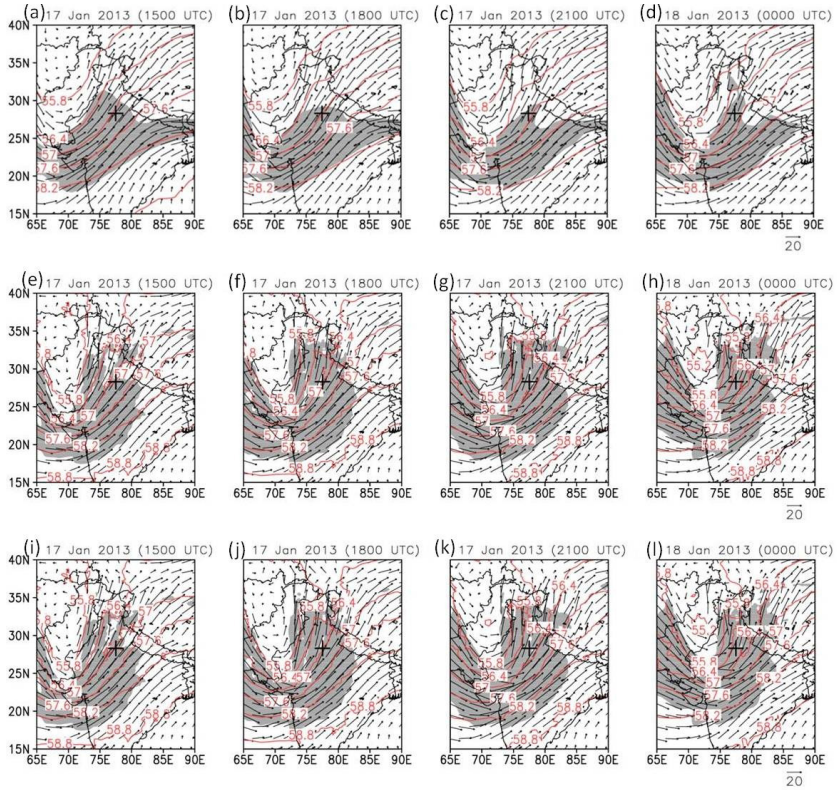

Figure 3. 500 hPa wind ($m\,s^{-1}$; vector), geopotential height (gpm × 100; contour) and wind speed ($m\,s^{-1}$; greater than 25 $m\,s^{-1}$ shaded in grey) from 15:00 UTC 17 January 2013 to 00:00 UTC 18 January 2013 at every three hours for **(a)–(d)** MERRA data, **(e)–(h)** model output with hail option and **(i)–(l)** model output with graupel option at 27 km horizontal model resolution. + Sign denoted NCR region.

NHESSD
2, 6033–6067, 2014

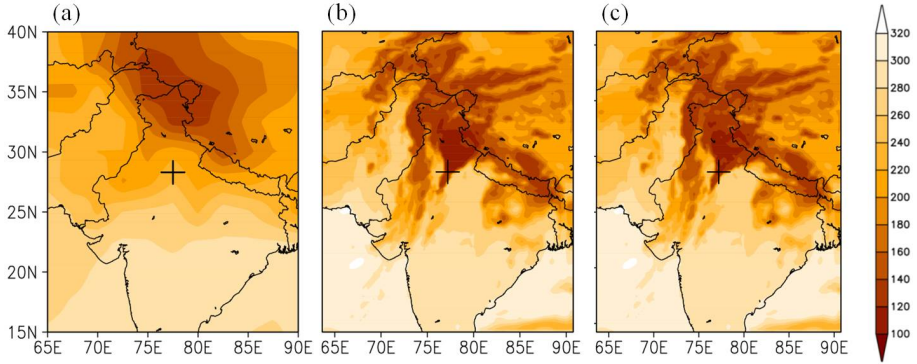

Figure 4. Daily mean OLR ($W\,m^{-2}$) at 17 January 2013 for **(a)** NOAA data, **(b)** model output with hail option and **(c)** model output with graupel option at 27 km horizontal model resolution. + Sign denoted NCR region.

NHESSD
2, 6033–6067, 2014

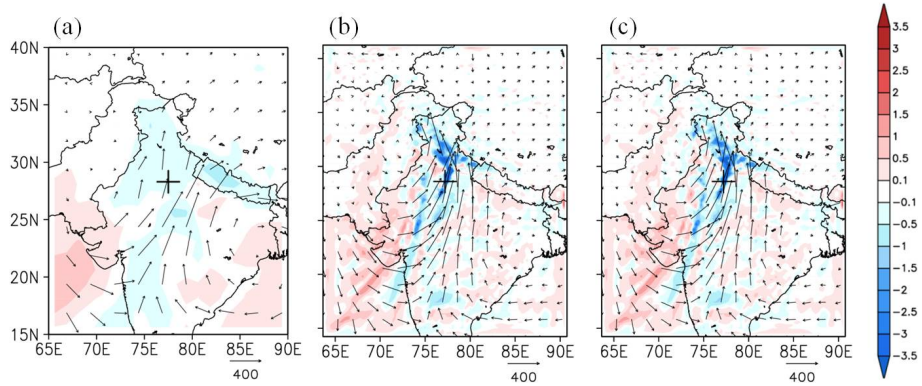

Figure 5. Vertical integrated moisture flux transport ($kg\,m^{-1}\,s^{-1}$; vector) and divergence ($\times 10^{-3}$ mm; shaded) at 15:00 UTC 17 January 2013 for **(a)** MERRA data, **(b)** model output with hail option and **(c)** model output with graupel option at 27 km horizontal model resolution. + Sign denoted NCR region.

NHESSD
2, 6033–6067, 2014

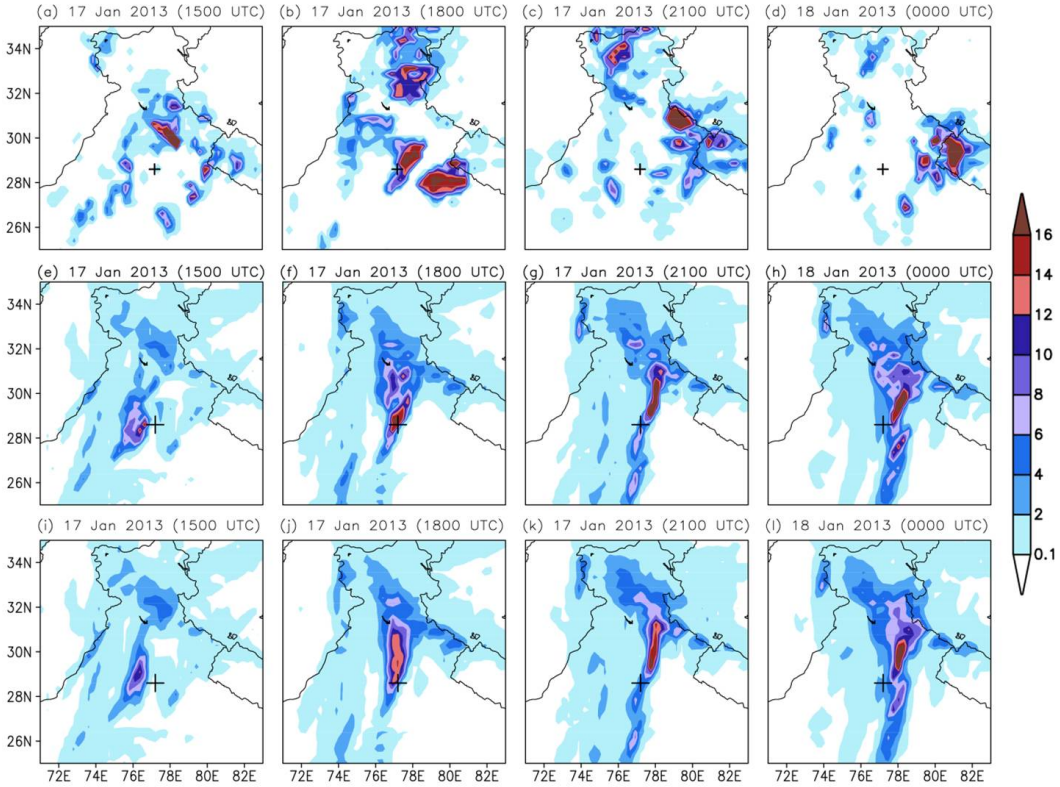

Figure 6. Precipitation (mm h^{-1}) from 15:00 UTC 17 January 2013 to 00:00 UTC 18 January 2013 **(a)–(d)** MERRA data, **(e)–(h)** model output with hail option and **(i)–(l)** model output with graupel option at 27 km horizontal model resolution. + Sign denoted NCR region.

NHESSD
2, 6033–6067, 2014

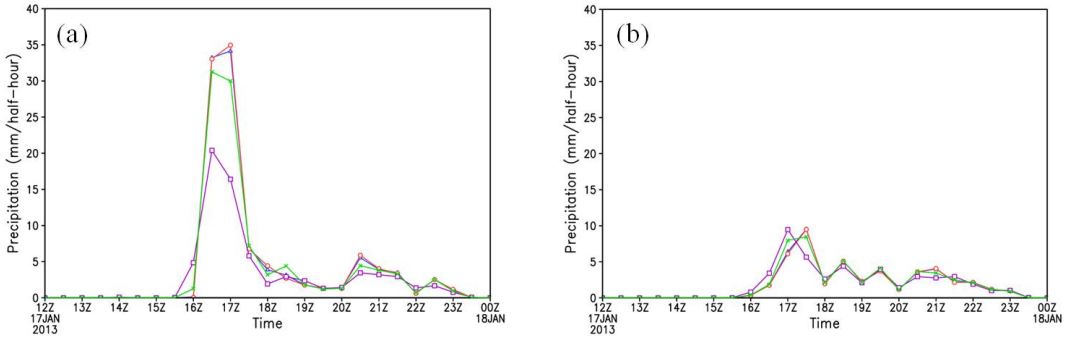

Figure 7. Precipitation (mm (half h)$^{-1}$) from 00:00 UTC 17 January 2013 to 00:00 UTC 18 January 2013 at NCR for **(a)** model output with hail option and **(b)** model output with graupel option; with 27 km horizontal model resolution (purple line with squares), 9 km resolution (green line with cross), 3 km resolution (blue line with triangle) and 1 km resolution (red line with circle).

NHESSD
2, 6033–6067, 2014

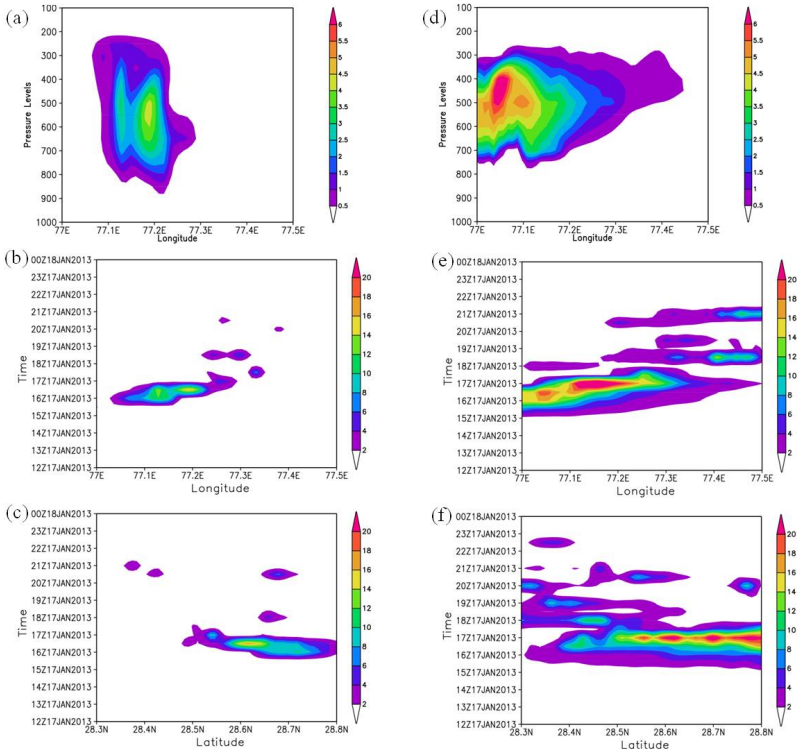

Figure 8. (a) Longitude-pressure cross section at latitude 28.6° N for model output at 1 km resolution at 16:00 UTC 17 January 2013 for hail mixing ratio (g kg^{-1}; shaded) with hail option, **(b)** longitude time cross section for model output at 1 km resolution at 16:00 UTC 17 January 2013 for vertical integrated hail mixing ratio (kg kg^{-1}; shaded) with hail option at latitude 28.6° N, **(c)** latitude time cross section for model output at 1 km resolution at 16:00 UTC 17 January 2013 for vertical integrated hail mixing ratio (kg kg^{-1}; shaded) with hail option at longitude 77.2° E and **(d)**–**(f)** same as **(a)**–**(c)** for graupel mixing ratio but with graupel option.

NHESSD
2, 6033–6067, 2014

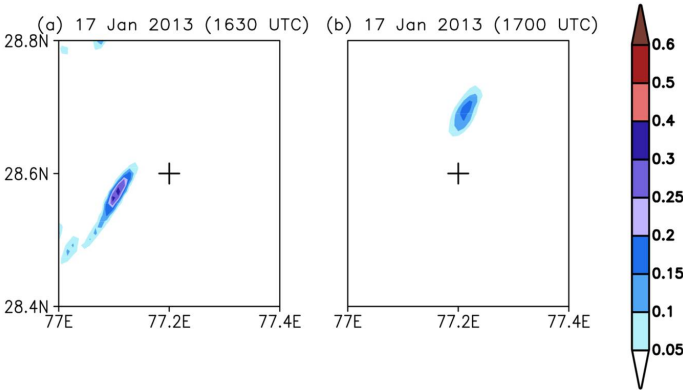

Figure 9. Hail precipitation (mm (half h)$^{-1}$) at 27 km horizontal model resolution with hail option for **(a)** 16:30 UTC 17 January 2013 and **(b)** 17:00 UTC 17 January 2013. + Sign denoted NCR.

NHESSD
2, 6033–6067, 2014

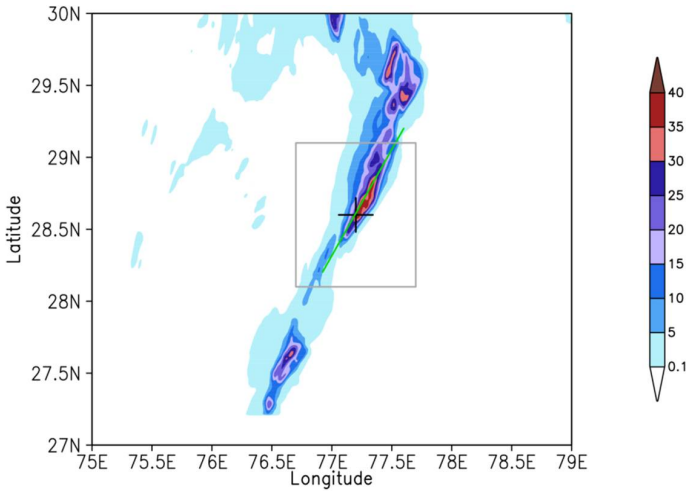

Figure 10. Model precipitation (mm (half h)$^{-1}$) at 17:00 UTC 17 January 2013 at 1 km horizontal model resolution with hail option. + Sign denoted NCR. (Green line drawn across maximum precipitation zone is along which vertical cross sections of various variables are analyzed and 1° × 1° grey box around NCR over which area averaged parameters are discussed in following sections.)

NHESSD
2, 6033–6067, 2014

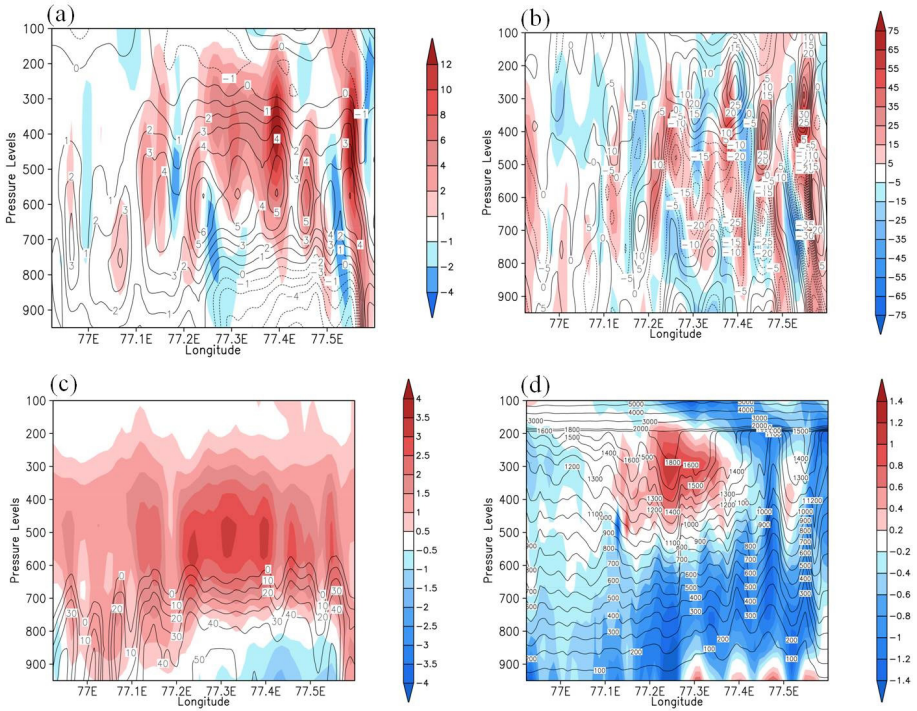

Figure 11. Longitude-pressure cross section (at the green line shown in Fig. 10) for model output with hail option at 1 km resolution at 17:00 UTC17 January 2013 for **(a)** vertical wind ($m\,s^{-1}$; shaded) and equivalent potential temperature (°C; contour), **(b)** relative vorticity ($\times 10^{-4}\,s^{-1}$; shaded) and divergence ($\times 10^{-4}$ mm; contour), **(c)** specific humidity anomaly (shaded) and reflectivity (dBZ; contour) and **(d)** geopotential height anomaly (shaded) and perturbation geopotential height (m; contour).

NHESSD
2, 6033–6067, 2014

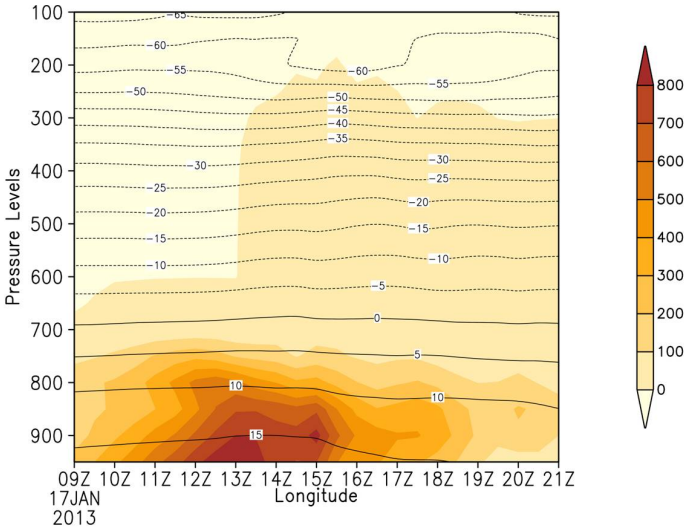

Figure 12. Time-pressure cross section (area averaged over the grey box shown in Fig. 10) at 1 km horizontal model resolution with hail option for CAPE ($J\,kg^{-1}$; shaded), temperature (°C; black contours) and specific humidity ($g\,kg^{-1}$; blue contours).

NHESSD
2, 6033–6067, 2014

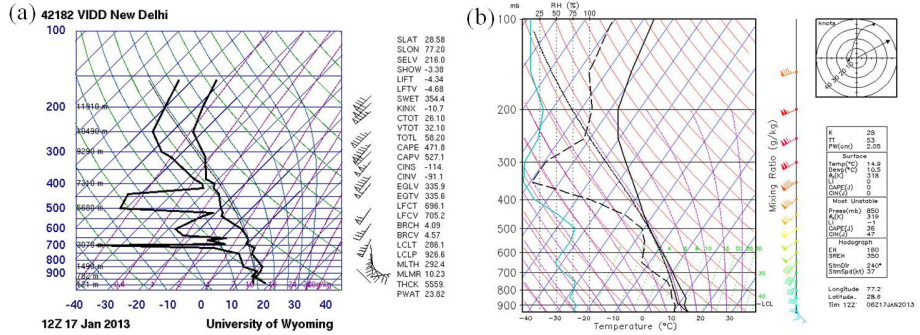

Figure 13. Sounding data at NCR at 12:00 UTC 17 January 2013 in graphical output for **(a)** observation and **(b)** 1 km horizontal model resolution with hail option.

NHESSD
2, 6033–6067, 2014

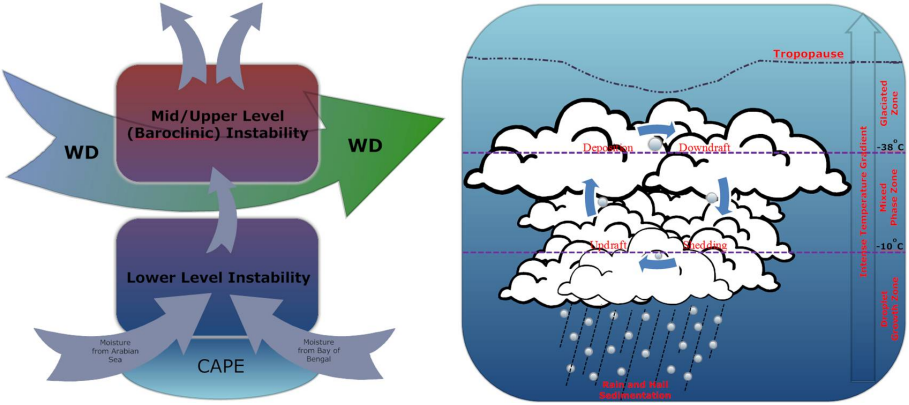

Figure 14. Conceptual model of the winter hailstorm.

NHESSD
2, 6033–6067, 2014